Generation of nanometer displacement using reduction mechanism consisting of torsional leaf spring hinges

Masato Hayashi[1] and Makoto Fukuda[1,#]

1 Department of Intelligent Machines and System Engineering, Graduate School of Science and Technology, Hirosaki University, 3 Bunkyo-cho, Hirosaki, Aomori-Pref, 036-8561, Japan
Corresponding Author / E-mail: fukuda@cc.hirosaki-u.ac.jp, TEL: +81-172-39-3678, FAX: +81-172-39-3678

Displacement reduction mechanisms using leverages that consist of elastic leaf springs and flexure hinges are widely used due to the high repeatability of positioning and the capability of linear motion. One application of the reduction mechanism is to provide a precise motion as a standard of nanometer displacement. However, large reduction rate exceeding 1/1000 has not been yet achieved because the leverage fulcrum cannot endure a large stress caused by the accumulated force in the mechanism. We have proposed a displacement reduction mechanism using torsional leaf spring hinges that can provide over 1/1000 reduction rate. The torsional hinge is made of two circular disks supported by four leaf springs as a solid construction. The hinge can provide an accurate twisting motion around the center of the disks and an accurate reduction motion without a leverage fulcrum deformation. This paper describes the performance of the displacement reduction system. One nanometer step displacement can be clearly distinguished at the reduction mechanism output and the transfer function of the reduction system in nanometer displacement is shown for verifying the dynamic characteristics. Furthermore several nanometer displacements such as sinusoidal, triangular and rectangular waves are demonstrated to show the capability of the reduction mechanism.

KEYWORDS : Nanometer displacement generation, Reduction mechanism, Torsional leaf spring hinge, Displacement standard

Manuscript received: January XX, 2011 / Accepted: January XX, 2011

1. Introduction

The guiding mechanisms that utilize leaf springs and flexure hinges are widely used due to the linearity and high stiffness. Most of the mechanisms provide either the magnified or reduced displacements when the structures are artfully devised based on leverages. One application of the linearity and large stiffness features is a dynamically controlled air journal bearing [1], which realized robust static stiffness in an air bearing by controlling the air outlet position with the flexure hinges and piezo-actuators. Another application is positioning stages of a single axis [2], two axes [3], three axes [4], or six axes [5], which were mainly achieved by magnifying the piezo-actuator displacement. On the other hand, the application of flexure hinge guides to the reduction displacement induced by an actuator is a few. Tamaru [6] studied the combination of the extending and reducing hinges for coarse and fine positioning control. And another important application of the reduction mechanism is to provide a precise motion as a standard of nanometer displacement. When a reduction displacement mechanism has a sufficient linearity to sub-nanometer, the mechanism makes it possible to provide the higher resolution than that the actuator possesses. For instance, using the reduction mechanism of 1/1000 reduction rate can provide 1-nm output displacement for 1-μm input displacement. Hama [7] designed a planer four-bar linkage mechanism to reduce the input motion aiming at 1/10000 reduction rate, but exact reduction rate could not be obtained due to the deformation of leverage fulcrums.

The fulcrum is a key element when a reduction mechanism is constructed of the accumulation of leverages. An ingenious elastic-hinge mechanism was proposed using torsion rods as a leverage fulcrum [8]. Although this mechanism has an advantage of the capability of large torsional deformation, the large deflection of the rod due to bending will also occur because the torsional rod diameter should be small to obtain the large deformation. Consequently, it is difficult to obtain the accurate rotation center by the use of this mechanism.

Then we propose the torsional leaf spring hinge that can provide both accurate rotational center and rigid flexure strength and the reduction mechanism of 1/1000 reduction rate using these hinges as fulcrums.

This paper describes the structure of the torsional leaf spring

hinge, the setup of the 1/1000 reduction mechanism, the performance of the reduction mechanism, and generating nanometer displacement for verifying the motional capability.

2. Torsional leaf spring hinge

The torsional leaf spring hinge (TLSH) consists of two circular plates supported by four leaf springs as shown in Fig. 1 (a) and (b). As the four leaf springs are independent each other, the deformation of the leaf spring is induced by the addition of the deflection and torsion of the leaf spring while two plates are twisted each other. This structure has an advantage of being able to provide both the strong deflection stiffness and the sensitive torsional stiffness.

When the deflection and the specific angle of torsion are shown as δ, θ, the bending force and torsional torque W, τ can be obtained by the following equations, respectively:

$$\mathbf{W} = 12\mathrm{EI}\frac{\delta}{\mathbf{c}^3} \qquad \cdots(1),$$

$$\tau = \frac{1}{3}\mathbf{G}\theta\mathbf{ab}^3 \qquad \cdots(2),$$

where E, I and c are the Young's modulus, the area moment of inertia, and the height of a leaf spring, and G, a, b are the modulus of transverse elasticity, the width and the thickness of a leaf spring.

Then the torsional torque T to twist two circular plates is obtained by the following equation:

$$\mathbf{T} = 4(\mathbf{r}\cdot\mathbf{W} + \tau) = \mathbf{r}\cdot 48\mathrm{EI}\frac{\delta}{\mathbf{c}^3} + \frac{4}{3}\mathbf{G}\theta\mathbf{ab}^3 \qquad \cdots(3),$$

where r is the radius from the center of the circular plate to that of the leaf spring.

This equation indicates that the torsional torque of TLSH is proportional to the deflection and the specific angle of torsion. This means the torsional leaf spring hinge can accurately rotate around a center when the leaf springs have the same spring constant. We made the TLSH from a stainless steel block as a solid construction by a wire-electric discharge machine.

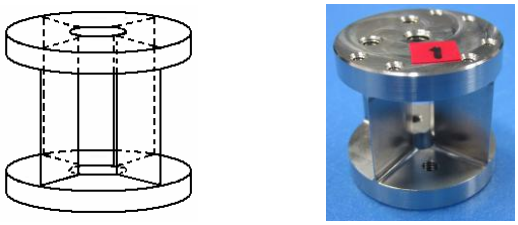

(a) Schematic chart of TLSH (b) Photograph of TLSH

Fig. 1 Torsional Leaf Spring Hinge consists of two circular plates and four leaf springs. (a) Schematic chart of TLSH, (b) Photograph of TLSH

The torsional stiffness of five TLSHs measured by the static methods is shown in Table 1. The static measurement method is to measure the displacement and torque of a lever mounted on the top circular plate of a TLSH when a torque is loaded on the lever. The individual difference of the torsional stiffness may be caused by the fluctuation of thickness in manufacturing.

Table 1 Torsional stiffness of torsional leaf spring hinges

TLSH No.	1	2	3	4	5
Static Stiffness [Nm/rad]	2.52	0.64	1.33	2.16	2.13

3. Displacement reduction mechanism

A displacement reduction mechanism is designed to perform the reduction rate of 1/1000, which can generate one nanometer output when one micrometer input. Figure 2 (a) shows the mechanism consisting of four TLSHs and four levers. The bottom plates of TLSH are mounted on a base plate and the top plates are connected with the levers. The torsional hinges are so aligned that the first lever can be twisted easily. The input force to TLSH is exerted in the circumference direction by a lever, and rotates the TLSH and the output deformation also comes up in the circumference direction with the reduction rate of the distance between a load and an effort point around the center.

The total reduction rate K is as follows:

$$\mathbf{K} = \frac{5}{40}\times\frac{5}{50}\times\frac{5}{50}\times\frac{40}{50} = \frac{1}{1000} \qquad \cdots(4),$$

where the numerator and the denominator show the output and input lever distances. The fractions show the reduction rate of each TLSH. The reason that the reduction rate of the last TLSH is smaller than that of the others is both to take an enough setup space for the capacitance sensor and to eliminate the measurement error induced by the lever inclination to the sensor.

Each lever is connected with a small steel ball to keep the contact point steady.

The experimental setup is shown in Fig. 2 (b). The input displacement is given by a piezo-actuator with a feedback of a strain gauge [9] in order to improve the repeatability and the response. The first lever is pushed by a steel ball on the top of the piezo-actuator. The displacement measurement is carried out by an electronic micrometer [10] with a wide range for the input and a capacitance displacement sensor [11] with a high resolution for the output. The reduction mechanism is mounted on a silicone gel vibration isolator on a vibration isolated table.

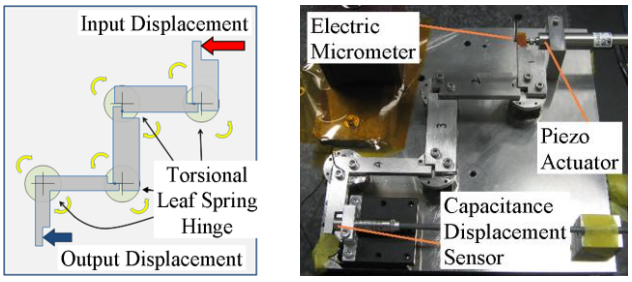

(a) Schematic chart (b) Experimental setup

Fig. 2 Displacement reduction mechanism utilizes torsional leaf spring hinges. (a) Schematic chart: The reduction rates are 5/40, 5/50, 5/50 and 40/50 from the input. (b) Experimental setup: a piezo-actuator is used as an input actuator, an electric displacement sensor and a capacitance displacement sensor are used for the input and output measurement, respectively.

4. Performance of the reduction mechanism

4.1 Performance of the piezo-actuator

A piezo-actuator with multilayer piezo ceramic stacks whose full range is 40 μm is used as an input actuator. In order to verify the linearity of the piezo-actuator displacement, the displacement with the feedback mode was measured by a digital micrometer [12]. The measurement was carried out at each 0.12 V for the range of 2.4 V (= 9.6 μm) in to-and-fro motion. The result is shown in Fig. 3 where the linearity of 3.98 μm/V and the maximum deviation of 0.11 μm from a line obtained by the least square method were yielded. This indicates that the actuator can be used for generating the input displacement.

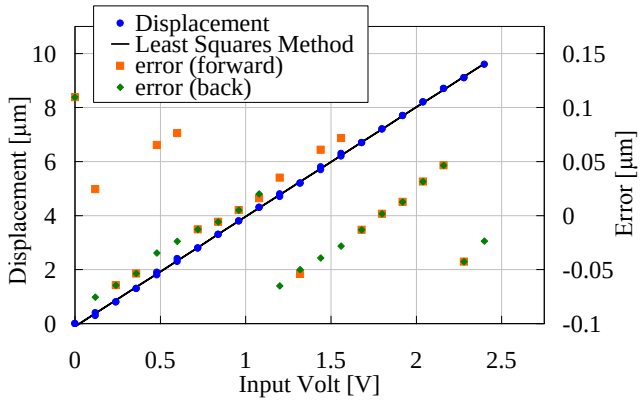

Fig. 3 Linearity of the piezo-actuator: the measurement is taken by digital micrometer in the piezo-actuator feedback mode. The error from the least square line is obtained. (Orange dots show the error in extending motion, green dots show the error in shortening motion.)

4.2 Step displacement performance of the reduction mechanism

To clarify the characteristics of the reduction mechanism, the response of the mechanism is investigated by giving the step displacement of 10 μm, 5 μm and 1 μm as input. For the 10-μm step and 5-μm step input, four steps and for the 1-μm step input, five steps were performed in to-and-fro motion with the interval of 5 sec. The input voltages were given by a pulse generator.

The results are shown in Fig. 4, Fig. 5, and Fig. 6. In the figures, the input displacement is shown as a red line on the right-hand y co-ordinate axis in [μm] unit, the maximum, the mean, and the minimum values of output displacements are shown as gray, blue, and green lines, respectively, on left-hand y co-ordinate axis in [nm] unit. To eliminate high frequency noise, the output from the capacitance sensor after the low-pass filter with 500 Hz cut-off frequency is used. The output has still a small vibration of 1.5 nm in the amplitude.

From 10-nm step and 5-nm step responses, the reduction of 1/1000 was achieved without backlash and hysteresis, as shown the output displacement corresponding to the input.

1-nm step response also shows the reduced displacement of 1/1000 without backlash and hysteresis, though a slight drift, which probably caused by air fluctuation, can be observed. In addition, 1-nm step displacement can be clearly distinguished by using the reduction mechanism.

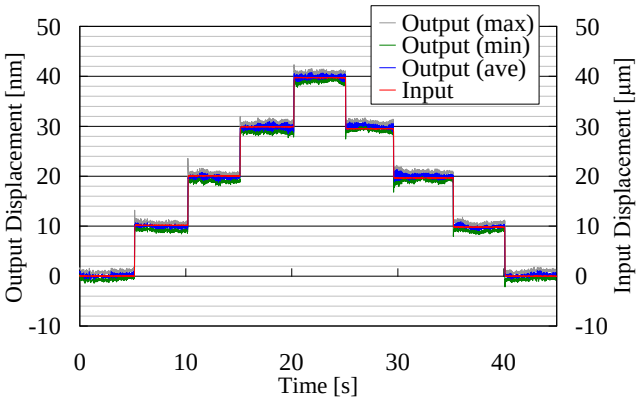

Fig. 4 Response of 10-nm step displacement

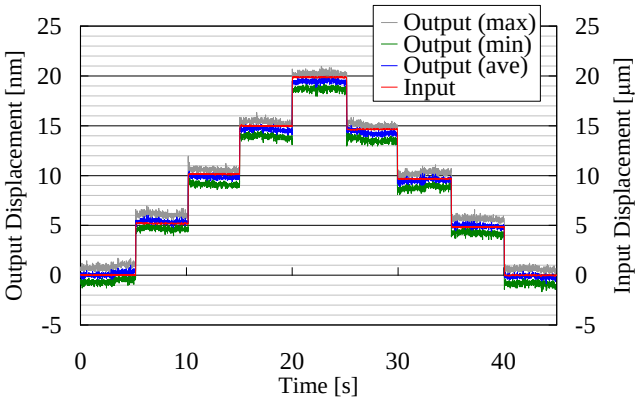

Fig. 5 Response of 5-nm step displacement

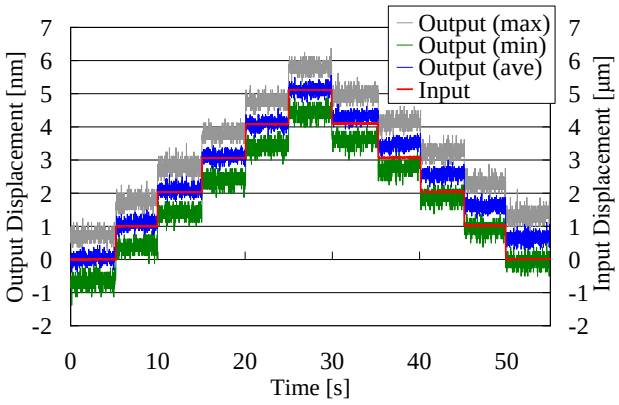

Fig. 6 Response of 1-nm step displacement

4.3 Dynamic characteristics of the reduction mechanism

To make the dynamic characteristic clear, the transfer function from the input to the output displacement of the reduction mechanism was measured. As the input was the voltage to the piezo-actuator and the output was the voltage of the capacitance displacement sensor without low-pass filter, the obtained transfer function includes the piezo-actuator, the reduction mechanism and the sensor. The input voltage was 1.25 V for piezo-actuator, which corresponds to 5 μm of the input displacement and 5 nm of the output displacement, and the frequency range was from 1 Hz to 1 kHz.

The result is shown in Fig. 7. The obtained gain and phase are shown as the upper and lower curves, respectively. The reduction mechanism has the dynamic characteristics whose gain has the flat response to 40 Hz and an antiresonant frequency at 160 Hz. From the variance of the phase, the phase delay can be appeared from 5 Hz and

the phase inversion is occurred at 400 Hz. The generating nanometer displacement capability of the mechanism is up to 80 Hz for the range of up to 3 dB down in the gain. Furthermore, this result indicates the transfer function analysis is available even in the nanometer displacement measurement.

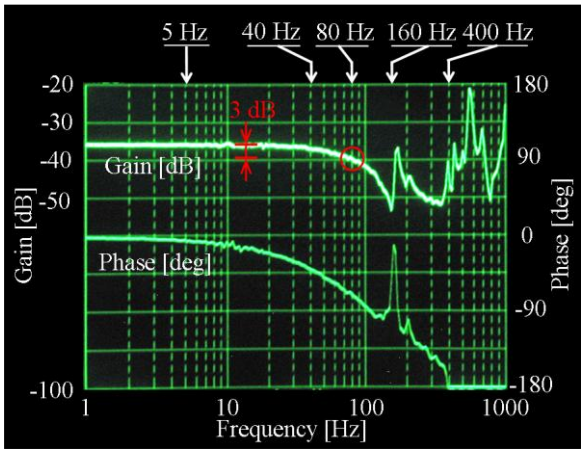

Fig. 7 Dynamic characteristics of the reduction mechanism: The upper and lower curves show the gain and phase of the transfer function from piezo-actuator input voltage to capacitance sensor output voltage.

5. Nanometer displacement generation

Various nanometer displacements, such as the sinusoidal, triangular and rectangular waves, are generated at various frequencies by the use of the reduction mechanism in order to demonstrate its motional capability. All of the amplitude of the input waves is 1.25 V uniformly, which corresponds to 5 μm for the input displacement and to 5 nm for the output displacement, to be compared easily.

The results of the nanometer displacement at the frequency of 5 Hz, 40 Hz and 80 Hz are shown in Fig. 8 - Fig. 10. The sinusoidal, triangular and rectangular wave responses are shown from upper to lower columns. In these figures, the red line shows the input displacement in [μm] unit at right-hand co-ordinate y axis, the blue line shows the output displacement in [nm] unit at left-hand co-ordinate y axis. The input displacement is converted from the input voltage to the piezo-actuator. Table 2 and Table 3 show the amplitude and phase delay at each frequency. Table 4, which is the step response, shows the delay time and the delay time ratio to the half period.

For the low frequency less than 5 Hz, all of the output displacements are coincident with that of the input one in both the amplitude and the phase. This means that the nanometer displacement can be generated using this reduction mechanism at the low frequency. But the higher is the frequency, the amplitude becomes smaller and the phase delay becomes larger as shown in Table 2 and 3. On the other hand, the rectangular response has a constant delay time of 2.6 ms for all the frequencies as shown in Table 4. This delay time includes the elapsed time to drive the piezo-actuator. The deformation of the rectangular response was caused by this delay time for all the frequencies.

From the results, the nanometer displacement can be accurately generated for the sinusoidal, triangular and rectangular input using the reduction mechanisms.

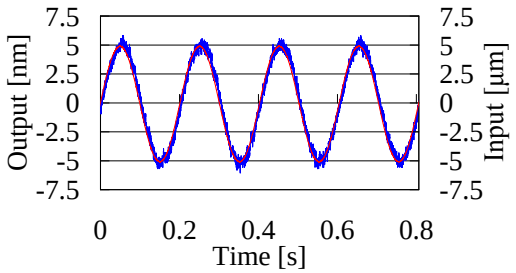

(a) 5 Hz

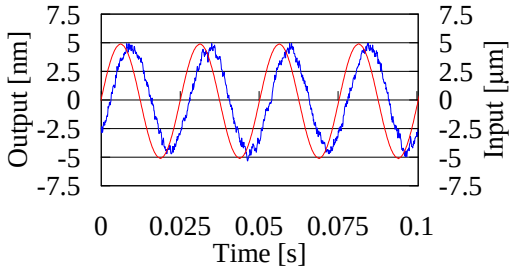

(b) 40 Hz

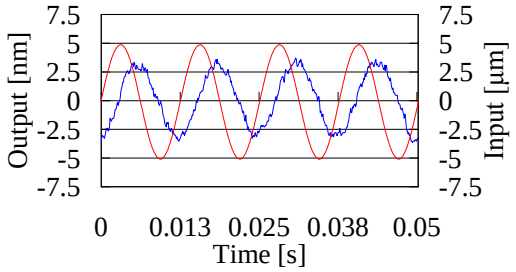

(c) 80 Hz

Fig. 8 Generating sinusoidal nanometer displacement

Table 2 Characteristics of sinusoidal wave generation

frequency	amplitude	phase delay
5 Hz	5.0 nm	0 deg
40 Hz	4.5 nm	-45 deg
80 Hz	3.5 nm	-80 deg

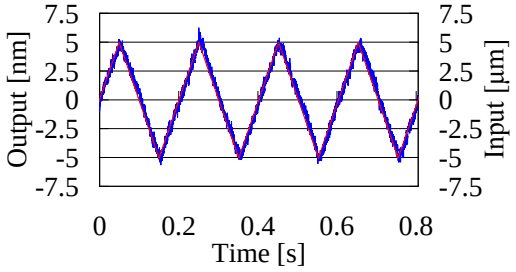

(a) 5 Hz

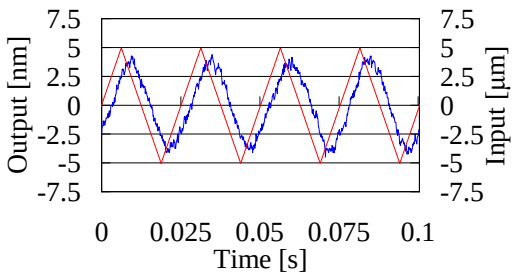

(b) 40 Hz

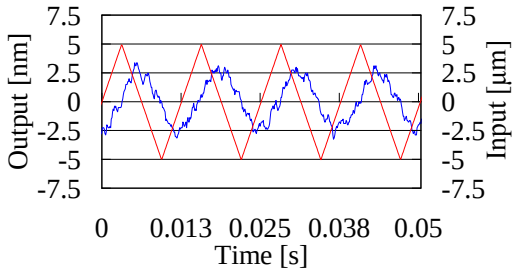

(c) 80 Hz

Fig. 9 Generating triangular nanometer displacement

Table 3 Characteristics of triangular wave generation

frequency	amplitude	phase delay
5 Hz	5.0 nm	0 deg
40 Hz	4.0 nm	-45 deg
80 Hz	3.0 nm	-80 deg

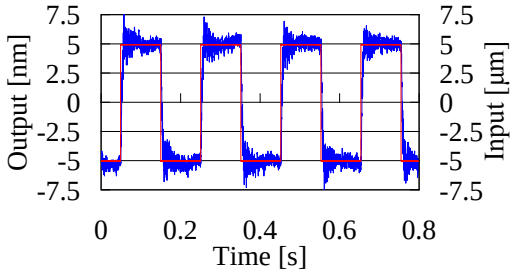

(a) 5 Hz

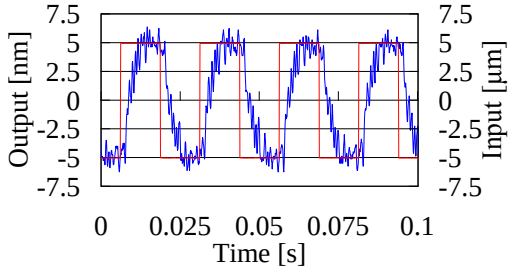

(b) 40 Hz

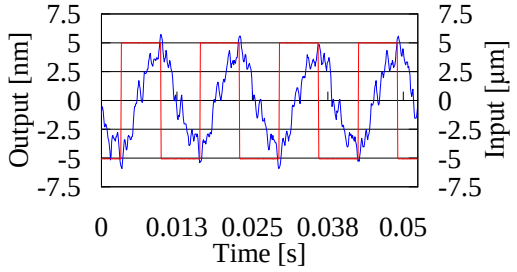

(c) 80 Hz

Fig. 10 Generating rectangular nanometer displacement

Table 4 Characteristics of rectangular wave generation

frequency	amplitude	delay time	half period	ratio of delay time to half period
5 Hz	5.0 nm	2.6 ms	100 ms	0.026
40 Hz	5.0 nm	2.6 ms	12.5 ms	0.208
80 Hz	5.0 nm	2.6 ms	6.25 ms	0.416

6. Conclusions

For the purpose of generating nanometer displacement in various wave forms, the reduction mechanism using the torsional leaf spring hinges as leverage fulcrums is proposed and investigated. The following results were obtained;

(1) The reduction mechanism can provide the reduction rate of 1/1000 without the backlash and hysteresis and one nanometer displacement was clearly distinguished for 1 μm input displacement.

(2) The transfer function analysis is available even in the nanometer displacement measurement to clarify the dynamic characteristics. The dynamic characteristics of the reduction mechanism had the dynamic response up to 80 Hz in 3 dB gain down from the transfer function measurement of 5 nm displacement.

(3) The reduction mechanism can generate the nanometer displacement of less than 5 nm in the sinusoidal, triangular and rectangular waves in the frequency range of less than 5 Hz.

ACKNOWLEDGEMENTS

This work was financially supported in part by an organization of Hirosaki University.

REFERENCES

[1] Shimokohbe A., Horikawa O., Sato K. and Sato H., “An active air journal bearing with ultraprecision, infinite static stiffness, high damping capability and new functions,” CIRP Annals - Manufacturing Technology, Vol. 40, No. 1, pp.563-566, January 1991.

[2] Yang R., Jouaneh M., Schweizel R., “Design and characterization of a low-profile micropositioning stage,” Precision Engineering, Vol. 18, No. 1, pp.20-29, January 1996.

[3] Yong Y. K., Aphale S. S., Reza Moheimani S. O., “Design, identification, and control of a flexure-based XY stage for fast nanoscale positioning,” IEEE Trans. Nanotechnology, Vol. 8, No. 1, pp. 46-54, January 2009.

[4] Zhang D., Chetwynd D.G., Liu X., Tian Y., “Investigation of a 3-DOF micro-positioning table for surface grinding,” International Journal of Mechanical Sciences 48, pp. 1401-1408, 2006

[5] Seugling R. M., LeBrun T., Smith S. T., Howard L. P., “A six-degree-of-freedom precision motion stage,” Review of scientific instrument, Vol. 73, No. 6, pp. 2462-2468, June 2002.

[6] Tamaru Y., Takafuji K., Shimizu H., “Cooperated positioning control for ultraprecision positioning in extended stroke path,” Trans. Jpn. Soc. Mech. Eng. Series C, Vol. 74, No. 745, pp. 2294-2300, Sep. 2008. (in Japanese)

[7] Hama A., Marushige T. and Nishimura K., “Study of design a reduction mechanism generating highly precise and accurate displacement,” Proc. of 1993 JSPE Spring Meeting, Tokyo, Japan, pp. 77-78, March 1993. (in Japanese)

[8] Oiwa T., and Matsnaga T., "A study on torsional elastic hinge," J. Jpn. Soc. Prec. Eng., Vol. 63, No. 10, pp.1454-1458, 1997. (in Japanese)

[9] Physik Instrumente (PI) GmbH & Co. KG, Auf der Römerstr. 1, D-76228 Karlsruhe/Palmbach, Germany

[10] Mahr GmbH Göttingen, Carl-Mahr-Str. 1, 37073 Göttingen, Germany

[11] MicroSense, LLC, 70 Industrial Avenue East, Lowell, Massachusetts 01852, USA

[12] Nikon Corporation, Shin-Yurakucho Bldg., 12-1, Yurakucho 1-chome, Chiyoda-ku, 100-8331 Tokyo, Japan